Supplementary Information for

Guiding Activity of Electrochemical Oxygen Evolution Reaction on Copper Oxide

Jiansen Wang[1,§], Jibiao Wang [1,§], Mengyuan Li[2], Houyu Zhu[3], Yuanxing Wang[1,*]

[1]State Key Laboratory of Green Papermaking and Resource Recycling, China-UK Low Carbon College, Shanghai Jiao Tong University, Shanghai 200240, China

[2]Guangzhou Customs District Technology Center, Guangzhou, Guangdong 510623, China

[3]Shandong Key Laboratory of Intelligent Energy Materials, School of Materials Science and Engineering, China University of Petroleum (East China), Qingdao, Shandong 266580, China

*Author to whom correspondence should be addressed: ywang19@alumni.nd.edu.

Computational details

All spin-polarized density functional theory (DFT) calculations were performed using the Vienna ab initio Simulation Package (VASP)[1, 2] with the GGA-PBE exchange-correlation functional.[3] Projected augmented wave (PAW)[4, 5] pseudopotentials were employed to model the ion cores, and a plane-wave cutoff energy of 500 eV was used. Periodic slab models were constructed to simulate the CuO(111) and Co_3O_4(111) surfaces. A vacuum region of 15 Å was introduced in the *z*-direction to minimize unwanted interactions between periodic cells. The dipole corrections were applied along the *z*-direction. Grimme's D3 method was adopted to consider the van der Waals (vdW) interactions.[6] The Hubbard + *U* approach was employed to alleviate the delocalization error of the GGA functional for treating transition metal atoms.[7] The values of U_{eff} have been set to around 3.3 and 7.0 eV for Co and Cu, respectively.[8]

The adsorption energies (E_{ads}) of adsorbate on the catalyst surface, such as *OH, *O, and *OOH, were calculated as:[9]

$$E_{ads} = E_{total} - E_{*} - E_{adsorbate} \quad (1)$$

where E_{total}, E_{*}, and $E_{adsorbate}$ represent the total energy of the adsorption system, catalyst surface, and adsorbate, respectively.

The change of Gibbs free energy (ΔG) was calculated based on the computational hydrogen electrode (CHE) model at 298.15 K:[9]

$$\Delta G = \Delta E_{DFT} + \Delta ZPE - T\Delta S \quad (2)$$

where ΔE_{DFT} is the adsorption electronic energy, while ΔZPE and $T\Delta S$ represent zero-point energy correction and entropy contribution. The data were post-processed using the VASPKIT tool.[10]

Experimental procedures

1. Chemicals

All reagents were used directly without further purification. Copper mesh (99.9%, 100 mesh), cobalt oxide (Co_3O_4, 99.5%, 50 nm), and potassium hydroxide (KOH, >99.99%) were purchased from Shanghai Aladdin Biochemical Technology Co., Ltd. Hydrochloric acid (HCl, AR, 36~38%) was purchased from Sinopharm Chemical Reagent Co., Ltd. Nafion solution (5 wt%) was obtained from J&K Scientific Ltd. The 1.0 mol L^{-1} HCl solution and 1.0 mol L^{-1} KOH electrolyte were prepared using deionized water.

2. Synthesis of CuO_x NWs

Copper mesh was cut into rectangular pieces (0.5 cm × 2.5 cm), ultrasonically cleaned in 1.0 mol L^{-1} HCl solution for 1 min to remove surface impurities and oxides, rinsed repeatedly with deionized water (3~4 times), and dried under an Ar stream. The dried mesh was immediately transferred to a muffle furnace and annealed at 600 °C in air for 4 h to obtain CuO_x NWs.[11]

3. Preparation of Co_3O_4 Catalyst

Approximately 10 mg of Co_3O_4 was dispersed in 2 mL of a mixed solution of isopropanol and deionized water (3:1 by volume). After 1 h of ultrasonication, 60 μL of 5 wt% Nafion was added, followed by another hour of ultrasonication to form a mixture. Drop 15.7 μL of the mixture on a 5 mm glassy carbon electrode and dry at room temperature. The catalyst loading was 0.4 mg cm^{-2}.[12]

4. Materials characterization

SEM measurements were performed using a field emission scanning electron microscope (JEOL JSM-7800F) at 0.01~30 kV. XRD patterns were collected using a Rigaku Smartlab SE X-ray diffractometer with a Cu Kα source (λ = 1.5406 Å). XPS

analysis was conducted on a Shimadzu AXIS SUPRA+ X-ray photoelectron spectrometer. All XPS spectra were calibrated to the C 1s peak (284.8 eV).

5. Electrochemical measurements

Electrochemical tests were carried out on a Biologic workstation using a standard three-electrode system with a 1.0 mol L^{-1} KOH electrolyte (pH = 14) at room temperature. The as-prepared catalyst electrode, a platinum sheet, and a Hg/HgO electrode (filled with 1.0 mol L^{-1} KOH) served as the working electrode, counter electrode, and reference electrode, respectively. All potentials were converted to the reversible hydrogen electrode (RHE) using Equation (3):

$$E\left(\text{vs. RHE}\right) = E\left(\text{vs. Hg/HgO}\right) + 0.098\ \text{V} + 0.0591\ \text{V} \times \text{pH} \tag{3}$$

Linear sweep voltammetry (LSV) was performed at a scan rate of 5 mV s^{-1}. Electrochemical double layer capacitance (Cdl) was determined by measuring cyclic voltammetry (CV) in the non-Faradaic interval (1.13~1.23 V vs. RHE) at scan rates of 20~100 mV s^{-1}. The current density was plotted against the scan rate of the CVs.[13] Tafel plots were generated via the steady-state approximation method: overpotential (η) was plotted against log$j$, and the reaction kinetics was determined by the Tafel slope.[14]

Table S1. Calculated total energies (E_{DFT}), zero-point energy (*ZPE*) corrections, and entropic contributions (*T*S*) to the Gibbs free energies (*G*) for OER catalyzed by CuO(111). All values are in eV units.

Species	*OH	*O	*OOH
E_{DFT}	-524.17	-518.05	-527.71
ZPE	0.38	0.06	0.44
*T*S*	0.06	0.06	0.11
G	-523.85	-518.05	-527.38

Table S2. Calculated total energies (E_{DFT}), zero-point energy (*ZPE*) corrections, and entropic contributions (*T*S*) to the Gibbs free energies (*G*) for OER catalyzed by Co_3O_4(111). All values are in eV units.

Species	*OH	*O	*OOH
E_{DFT}	-680.06	-675.07	-683.81
ZPE	0.34	0.05	0.45
*T*S*	0.12	0.03	0.15
G	-679.84	-675.06	-683.51

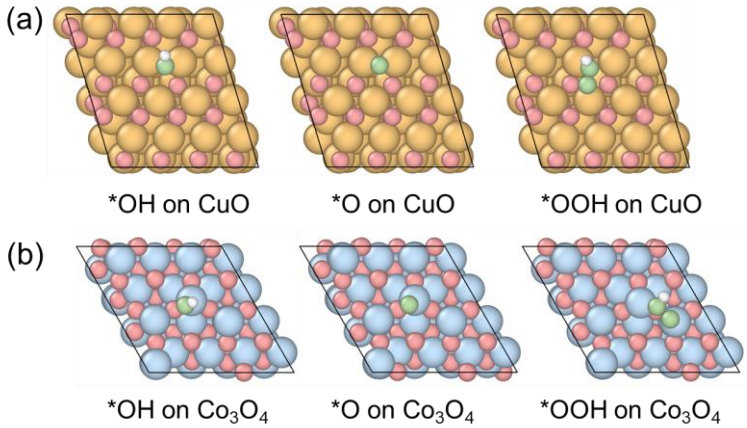

Figure S1. Top view of intermediate geometries for the OER catalyzed by (a) CuO(111) and (b) Co_3O_4(111). (Cu: yellow, Co: blue, O in catalyst: pink, O in intermediate: green, H: white)

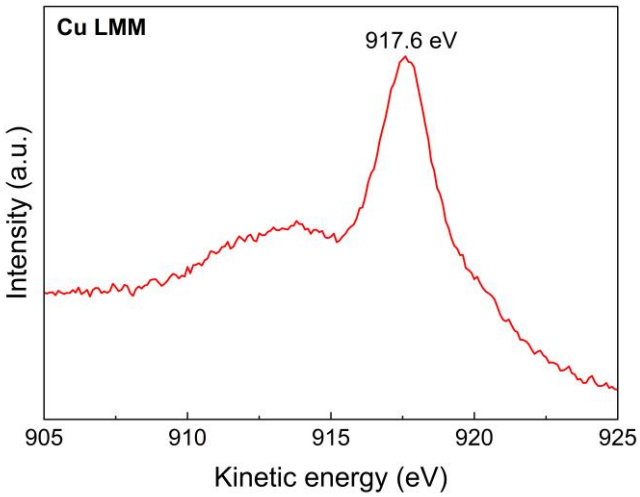

Figure S2. Cu LMM photoelectron spectrum of the CuO_x NWs.

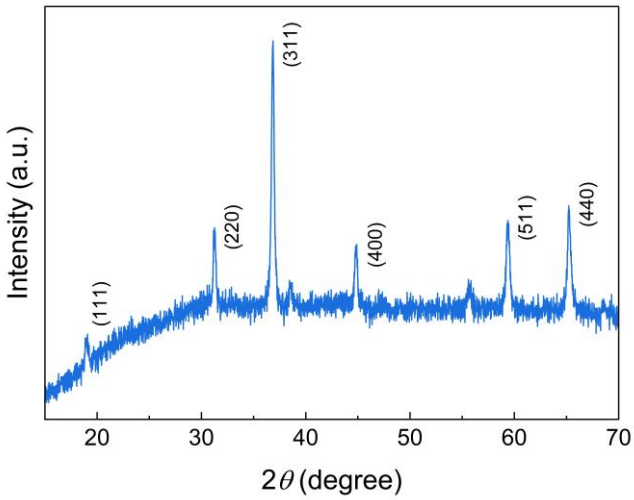

Figure S3. XRD pattern of the commercial Co_3O_4 NPs.

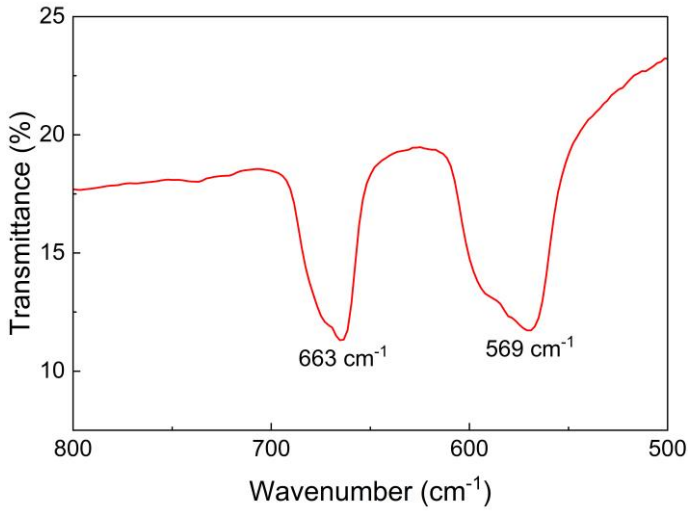

Figure S4. FT-IR spectrum of the commercial Co_3O_4 NPs.

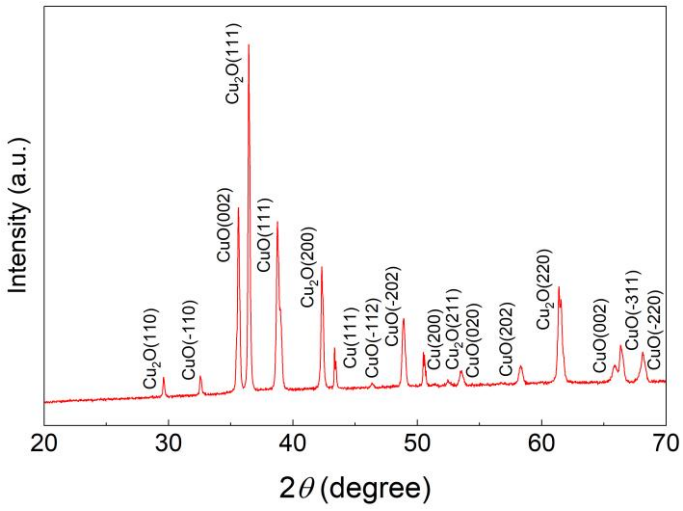

Figure S5. XRD pattern of the CuO_x NWs after the OER.

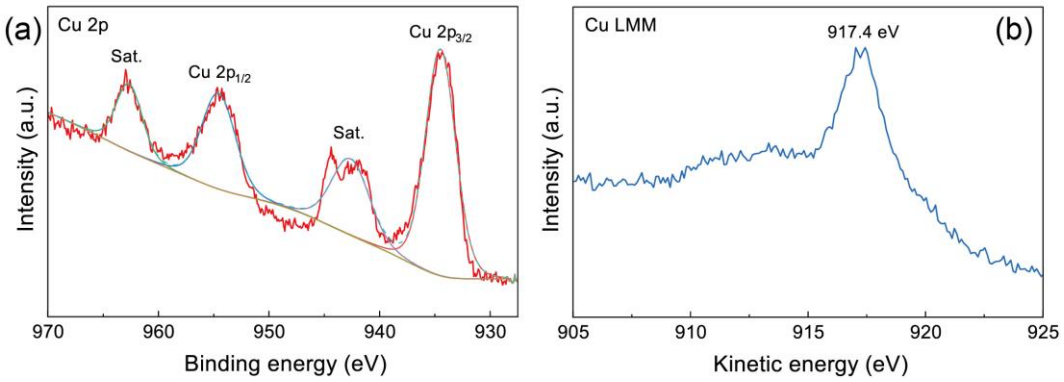

Figure S6. Cu 2p (a) and Cu LMM (b) photoelectron spectrum of the CuO_x NWs after the OER.

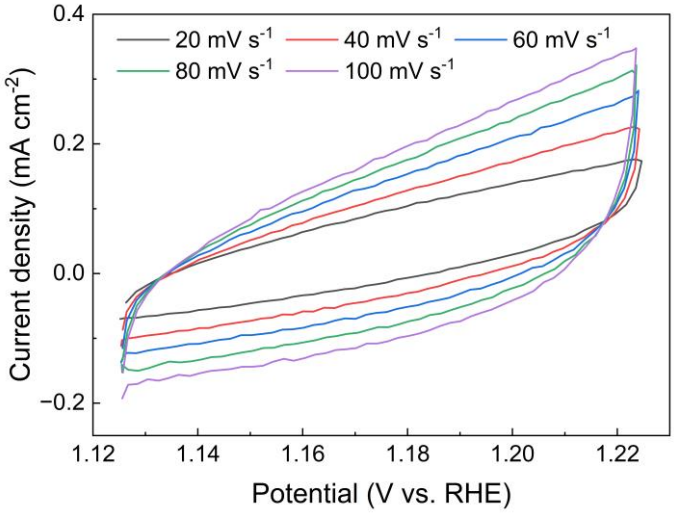

Figure S7. CVs taken on the CuO_x NWs over a range of scan rates in a potential window where double-layer charging and discharging are relevant.

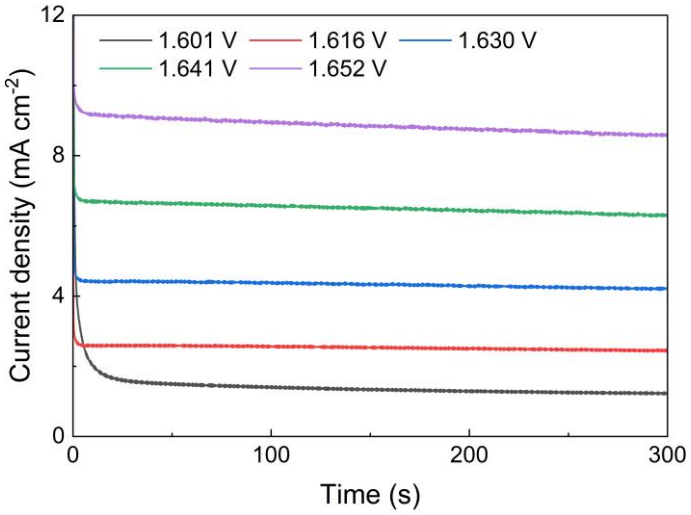

Figure S8. Steady-state electrochemical *j-t* plots of oxygen evolution on the CuO_x NWs for Tafel analysis.

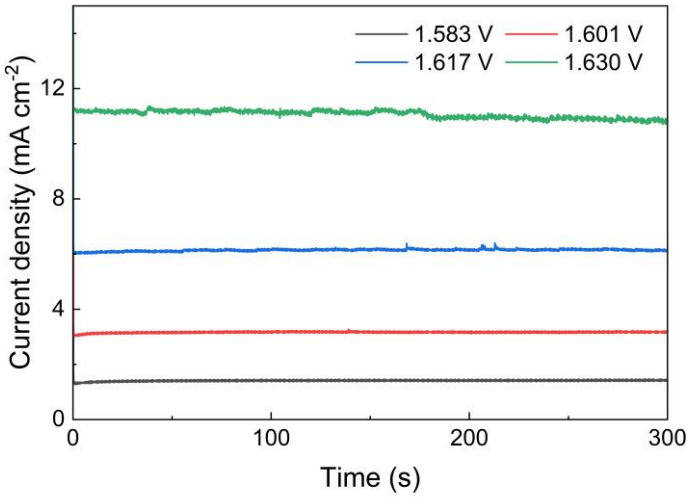

Figure S9. Steady-state electrochemical *j-t* plots of oxygen evolution on the Co_3O_4 NPs for Tafel analysis.

References

(1) Kresse, G.; Furthmüller, J. Efficiency of ab-initio total energy calculations for metals and semiconductors using a plane-wave basis set. *Comput. Mater. Sci.* **1996**, *6*, 15-50.

(2) Kresse, G.; Furthmüller, J. Efficient iterative schemes for ab initio total-energy calculations using a plane-wave basis set. *Phys. Rev. B* **1996**, *54*, 11169-11186.

(3) Perdew, J. P.; Burke, K.; Ernzerhof, M. Generalized Gradient Approximation Made Simple. *Phys. Rev. Lett.* **1996**, *77*, 3865-3868.

(4) Blöchl, P. E. Projector augmented-wave method. *Phys. Rev. B* **1994**, *50*, 17953-

17979.
(5) Kresse, G.; Joubert, D. From ultrasoft pseudopotentials to the projector augmented-wave method. *Phys. Rev. B* **1999**, *59*, 1758-1775.
(6) Grimme, S. Semiempirical GGA-type density functional constructed with a long-range dispersion correction. *J. Comput. Chem.* **2006**, *27*, 1787-1799.
(7) Dudarev, S. L.; Botton, G. A.; Savrasov, S. Y.; Humphreys, C. J.; Sutton, A. P. Electron-energy-loss spectra and the structural stability of nickel oxide: An LSDA+U study. *Phys. Rev. B* **1998**, *57*, 1505-1509.
(8) Niu, W.; Shi, J.; Ju, L.; Li, Z.; Orlovskaya, N.; Liu, Y.; Yang, Y. Understanding Synergism of Cobalt Metal and Copper Oxide toward Highly Efficient Electrocatalytic Oxygen Evolution. *ACS Catal.* **2018**, *8*, 12030-12040.
(9) Nørskov, J. K.; Bligaard, T.; Logadottir, A.; Kitchin, J. R.; Chen, J. G.; Pandelov, S.; Stimming, U. Trends in the Exchange Current for Hydrogen Evolution. *J. Electrochem. Soc.* **2005**, *152*, J23.
(10) Wang, V.; Xu, N.; Liu, J.-C.; Tang, G.; Geng, W.-T. VASPKIT: A user-friendly interface facilitating high-throughput computing and analysis using VASP code. *Comput. Phys. Commun.* **2021**, *267*, 108033.
(11) Wang, Y.; Niu, C.; Zhu, Y.; He, D.; Huang, W. Tunable Syngas Formation from Electrochemical CO_2 Reduction on Copper Nanowire Arrays. *ACS Appl. Energy Mater.* **2020**, *3*, 9841-9847.
(12) Zhang, R.; Pan, L.; Guo, B.; Huang, Z.-F.; Chen, Z.; Wang, L.; Zhang, X.; Guo, Z.; Xu, W.; Loh, K. P.; Zou, J.-J. Tracking the Role of Defect Types in Co_3O_4 Structural Evolution and Active Motifs during Oxygen Evolution Reaction. *J. Am. Chem. Soc.* **2023**, *145*, 2271-2281.
(13) Li, C. W.; Kanan, M. W. CO_2 Reduction at Low Overpotential on Cu Electrodes Resulting from the Reduction of Thick Cu_2O Films. *J. Am. Chem. Soc.* **2012**, *134*, 7231-7234.
(14) Anantharaj, S.; Noda, S.; Driess, M.; Menezes, P. W. The Pitfalls of Using Potentiodynamic Polarization Curves for Tafel Analysis in Electrocatalytic Water Splitting. *ACS Energy Lett.* **2021**, *6*, 1607-1611.